Journal of Applied Geophysics 99 (2013) 42–50

Contents lists available at ScienceDirect

Journal of Applied Geophysics

journal homepage: www.elsevier.com/locate/jappgeo

A robust method for microseismic event detection based on automatic phase pickers

Juan I. Sabbione *, Danilo R. Velis *,*

Facultad de Ciencias Astronómicas y Geofísicas, UNLP, Paseo del Bosque s/n, 1900 La Plata, Argentina
CONICET, Argentina

ARTICLE INFO

Article history:
Received 4 February 2013
Accepted 27 July 2013
Available online 6 August 2013

Keywords:
Microseism
Automatic detection
Picking

ABSTRACT

We present a robust method for the automatic detection and picking of microseismic events that consists of two steps. The first step provides accurate single-trace picks using three automatic phase pickers adapted from earthquake seismology. In the second step, a multi-channel strategy is implemented to associate (or not) the previous picks with actual microseismic signals by taking into account their expected alignment in all the available channels, thus reducing the false positive rate. As a result, the method provides the number of declared microseismic events, a confidence indicator associated with each of them, and the corresponding traveltime picks. Results using two field noisy data records demonstrate that the automatic detection and picking of microseismic events can be carried out with a relatively high confidence level and accuracy.

© 2013 Published by Elsevier B.V.

1. Introduction

Microseismicity studies have become an essential tool in nowadays oil reservoir geophysics (Kendall et al., 2011) and geological carbon dioxide (CO_2) storage (Oye et al., 2012; Verdon, 2011). In oil secondary recovery, high-pressure fluid injection is used to promote or to enhance the gas/oil production. This generates microfractures in the vicinity of the reservoir whose spatio-temporal distribution needs to be monitored for better controlling both the injection process and the development of the reservoir (Maxwell, 2011; Maxwell and Urbancic, 2001). In some cases, these processes require a real-time mapping of the microseisms' hypocenters, where efficiency and reliability are crucial for taking cost-effective decisions. Usually, both P- and S-waves arrival times and an approximate velocity model are needed to derive accurate hypocenter locations. Therefore, the automatic detection of microseisms and accurate picking of the associated traveltimes are of paramount importance for the monitoring of the induced hydraulic fracturing processes.

Microseismic monitoring is frequently carried out by placing triaxial-geophone arrays within one or more monitoring wells in the nearby of the extraction well. Thus, a few hours long continuous records are obtained in order to detect the occurrence of microfractures. Alternatively, when nearby wells are not available, geophone arrays may be placed along the surface. In the former case, the arrays typically consist of 8 to 12 geophones, and so the records consist of 24 to 36 channels, respectively. On the other hand, when using surface arrays, the number of receivers may be as large as several thousands (Duncan, 2012). Both scenarios give rise to large data volumes with low signal-to-noise ratios, specially when hypocenters are deep and distant from the monitoring array. One key issue that also explains the low signal quality is that microseisms induced by hydraulic injection are characterized by very small magnitudes (Shemeta and Anderson, 2010). Moreover, depending on the polarization pattern arriving to the receivers, the signal may be partially or totally masked by noise in one or two of the three components. Consequently, one of the main challenges when processing microseismic data is not only to automatically detect the actual microseismic signal arrivals precisely, but also to avoid the picking of false events.

Since microseisms caused by hydraulic fracturing are interpreted as "tiny" earthquakes, automatic phase pickers can be used to process microseismic data (Sabbione and Velis, 2012). In global seismology, the most common approach to detect the advent of a given phase is to compute certain attribute or "characteristic function" (CF), which is devised to enhance the signal changes, and calculate its average within two time-windows of different sizes: the short-term average (STA) and the long-term average (LTA). Then, an event is declared when the ratio between these two terms exceeds a given threshold value, giving rise to the so-called STA/LTA methods (Allen, 1982). The preceding approach has already been used to detect microseisms by different authors. Munro (2004) developed an algorithm in which the averaged attribute is the energy. Similarly, Chen and Stewart (2006) used a characteristic function based on the trace absolute values. Recently, Wong et al. (2009) presented the "modified energy ratio" method (MER), which is validated comparing it to a classical STA/LTA algorithm. The window scheme in the MER is similar to the one used by Earle and

* Corresponding authors. Tel.: +54 2214239593.
** Correspondence to: J.I. Sabbione, Facultad de Ciencias Astronómicas y Geofísicas, UNLP, Paseo del Bosque s/n, 1900 La Plata, Argentina. Tel.: +54 2214239593.
E-mail addresses: jsabbione@fcaglp.unlp.edu.ar (J.I. Sabbione), velis@fcaglp.unlp.edu.ar (D.R. Velis).

0926-9851/$ – see front matter © 2013 Published by Elsevier B.V.
http://dx.doi.org/10.1016/j.jappgeo.2013.07.011

Shearer (1994) to detect earthquake phases, but the chosen attributes and criteria for selecting the window lengths are different. More recently, Vera-Rodriguez et al. (2011) presented a new method in which the time picks are obtained using blocky STA/LTA curves recovered from inversion with a sparsity constraint.

In this work we present a simple and robust technique to detect microseismic events and pick their arrival times automatically that works well even under noisy conditions. Our method consists of two steps and is applied to data collected at a monitor well. First, potential events and their corresponding traveltimes are determined based on three automatic phase pickers that proved to be specially adequate to process global seismology data (Sabbione, 2012). The time picks are obtained using either the Earle and Shearer's method (Earle and Shearer, 1994), or some modifications to the Allen's method (Allen, 1978) or the Baer and Kradolfer's method (Baer and Kradolfer, 1987). Secondly, a multi-trace strategy is proposed to declare a microseism (or not) based on number of the picks obtained in the previous step using a fixed-length (moving) search window. As a result, the number of declared microseisms, an indicator of the confidence associated with each of them, and the arrival times for those traces in which the microseism is detected are obtained automatically. The results using two field datasets show that the proposed method performs very well, providing accurate traveltimes and reliable detections with no false alarms.

In what follows, we first describe the theory and methods we propose to detect microseismic events and pick their arrival times automatically. In this sense, we present the three automatic phase picker algorithms used to scan each trace of the record looking for potential microseism arrivals. Also, the multi-trace approach devised to asses the presence (or not) of a microseism together with a confidence indicator are justified and depicted in order to complete the methodology description. Next, the proposed strategy is illustrated using two field data records with regular and poor signal-to-noise ratios, respectively. Then, we provide a discussion to interpret the results and point out the main contributions of our method. Finally, we enumerate the conclusions of this work.

2. Theory and methods

2.1. Trace-by-trace picking

The first step of the proposed approach is a trace-by-trace process based on one of the three automatic phase pickers: (1) the method presented by Earle and Shearer (1994), (2) the classical method introduced by Allen (1978), and (3) the method proposed by Baer and Kradolfer (1987). These algorithms were borrowed from earthquake seismology and were selected regarding its better performance compared to other autopickers (Sabbione, 2012). The three methods, together with the proposed modifications, are briefly described below.

2.1.1. Earle and Shearer's method (ESM)

In this method, the characteristic function is given by the envelope of the signal ES_i and is computed via

$$ES_i = \sqrt{s_i^2 + \tilde{s}_i^2}, \tag{1}$$

where s_i is the i-th sample of the signal (seismogram) and $\tilde{s}_i$ its Hilbert transform. Then, ES_i is averaged within two consecutive moving windows of lengths T_{STA} and T_{LTA}, respectively, with $T_{LTA} > T_{STA}$. Thus, the STA/LTA ratio is obtained by means of

$$\frac{\mathrm{STA}_i}{\mathrm{LTA}_i} = \frac{\frac{1}{N_{STA}}\sum_{j=i}^{i+N_{STA}-1} ES_j}{\frac{1}{N_{LTA}}\sum_{j=i-N_{LTA}}^{i-1} ES_j}, \tag{2}$$

where N_{STA} and N_{LTA} are the corresponding lengths of the non-overlapping windows.

To avoid rapid fluctuations that may lead to wrong picks, a low-pass Hanning filter is used to smooth the results. Finally, the events are declared when the smoothed STA/LTA ratio exceeds a given threshold *THR*, and the arrival times are picked at the inflection point that immediately precedes the maximum of the STA/LTA ratio. The Earle and Shearer's method is depicted in Fig. 1.

2.1.2. Modified Allen's method (MAM)

This STA/LTA method is based on the classical approach presented by Allen (1978), who proposed to calculate the characteristic function as

$$CF_i = s_i^2 + C_i(s_i - s_{i-1})^2, \tag{3}$$

with

$$C_i = \frac{\sum_{j=1}^{i}|s_j|}{\sum_{j=1}^{i}|s_j - s_{j-1}|}. \tag{4}$$

Note that C_i is a weighting factor that balances the two terms of CF_i: the first one related to the signal energy, and the second one to the signal frequency.

Next, we modify the classical Allen's method: in the MAM, we use the same window scheme as in the ESM (see Fig. 2b). Thus, the STA/LTA ratio is computed by replacing ES_j with CF_j into Eq. (2), and then it is assigned to the first sample of the window ahead in time. After smoothing the STA/LTA ratio using a Hanning filter, an event is declared when this smoothed ratio exceeds a given threshold *THR*. Finally, the arrival times are picked at the corresponding local maxima, as shown in Fig. 2c.

2.1.3. Modified Baer and Kradolfer's method (MBKM)

The method proposed by Baer and Kradolfer (1987) relies on an approximation of the envelope function E_i^2 given by:

$$E_i^2 = s_i^2 + \frac{\sum_{j=1}^{i} s_j^2}{\sum_{j=1}^{i}\left(s_j - s_{j-1}\right)^2}(s_i - s_{i-1})^2. \tag{5}$$

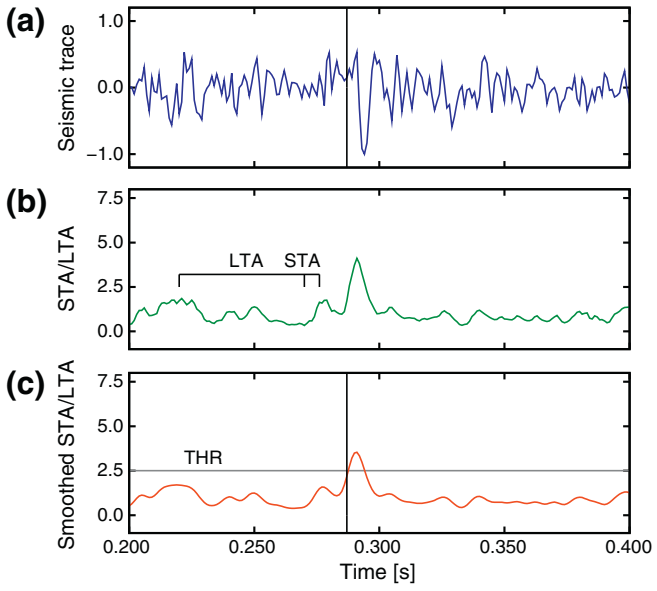

Fig. 1. ESM: (a) Normalized seismic trace and final pick (vertical line). (b) STA/LTA ratio and window scheme. (c) Smoothed STA/LTA ratio and final pick at the inflection point that precedes the maximum above THR.

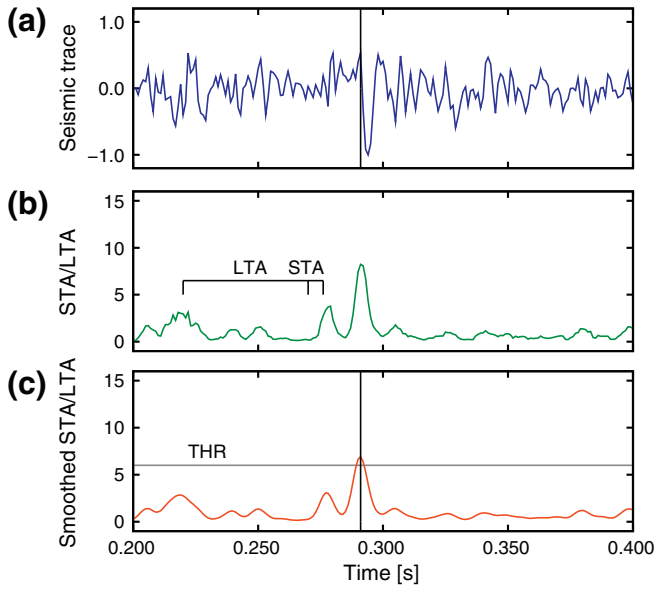

Fig. 2. MAM: (a) Normalized seismic trace and final pick (vertical line). (b) STA/LTA ratio and window scheme. (c) Smoothed STA/LTA ratio and final pick at the maximum above *THR*.

Instead of averaging E_i^2 within two time windows as in a STA/LTA method, Baer and Kradolfer (1987) proposed to calculate the normalized squared envelope function for each sample i along the trace:

$$BK_i = \frac{E_i^4 - \widetilde{\mu}_{E_i^4}}{\widetilde{\sigma}_{E_i^4}}, \tag{6}$$

where $\widetilde{\mu}_{E_i^4}$ represents the estimated mean value of E_i^4 and $\widetilde{\sigma}_{E_i^4}$ its estimated standard deviation. This quantity is shown in Fig. 3b. As in the previous two methods, and in order to avoid rapid fluctuations of *BK*, we use a low-pass Hanning filter, which was not used in the original algorithm. Then, events are declared if the smoothed *BK* exceeds a given threshold *THR*. Finally, the arrival times are picked at the first sample that exceeds *THR*, as shown in Fig. 3c.

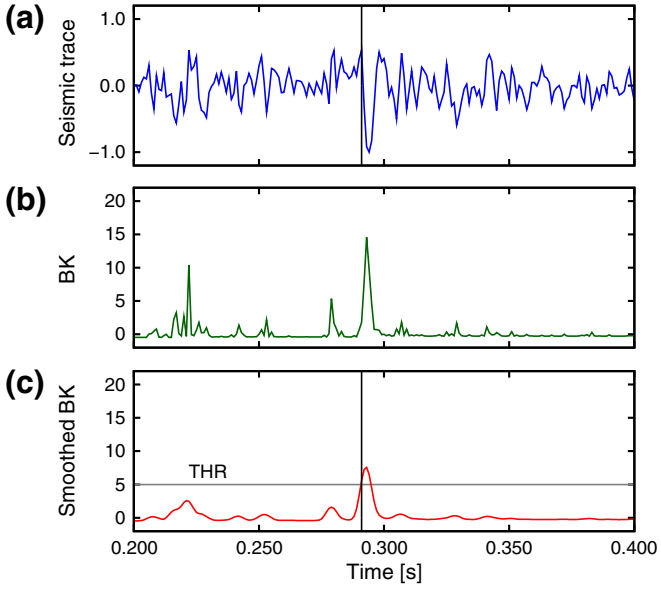

Fig. 3. MBKM: (a) Normalized seismic trace and final pick (vertical line). (b) *BK* as computed using Eq. (6). (c) Smoothed *BK* and final pick at the first sample exceeding *THR*.

2.2. The microseism hyperbola

To introduce the multi-channel strategy, let us first consider a typical microseismic monitoring scenario, as shown in Fig. 4a. The figure depicts a two-dimensional medium with constant velocity v and a vertical array of receivers placed at a few hundred meters from the expected micro-earthquake locations. If (x,z) is the (unknown) source location, τ its occurrence time, and (x_g,z_g) are the receivers coordinates, the arrival times of the microseismic signal are given by:

$$t(z_g) = \tau + \sqrt{\frac{(x_g - x)^2}{v^2} + \frac{(z_g - z)^2}{v^2}}. \tag{7}$$

Eq. (7), which represents an apex-shifted hyperbola in the time vs. depth domain, can be rewritten as

$$t(z_g) - \tau = t_0 \sqrt{1 + \left(\frac{z_g - z}{x_g - x}\right)^2}, \tag{8}$$

where $t_0 = (x_g - x)/v$ is a constant that represents the traveltime that would be recorded if $z_g = z$. Clearly, if $|z_g - z| \ll |x_g - x|$, the propagation time given by Eq. (8) is almost constant, and thus the microseismic arrivals are expected to align along quasi-horizontal low-curvature hyperbolas, as shown in Fig. 4b. Model parameters of Fig. 4a resemble the real data examples we are going to show in the following sections. In this case, a fairly short time moving window (50 ms) should cover, for a particular microseism, the microseismic arrivals in all channels (see Fig. 4b). Our criterion for the detection of events is based on this simple idea.

2.3. Multi-trace approach and declaration of microseisms

With the motivation given in the previous section, and once all the potential events were picked using one of the trace-by-trace processes described previously, we then count, for each time step of a moving window of fixed size, the number of picks that fall within it. This search window is illustrated in Fig. 5. The picks were obtained using the MAM algorithm. For the sake of simplicity, traces are numbered from 1 to 24, where the *x*-, *y*- and *z*-components correspond to traces 1–8, 9–16 and 17–24, respectively. Note that for traces 1, 2, 3, 9, 10, 13, 14 and 24 no event was detected, while two picks were assigned to traces 6 and 21. In these last two cases, one of the picks corresponds to the actual microseism, and the other one is a "false positive" pick. In the rest of the traces, all the picks can be associated to the actual microseism.

A microseism is declared if any component in the search window contains at least one pick in at least half of the traces (4 traces in our data examples, which are given by 8-channels arrays). Clearly, the larger the search window length, the smaller the risk of missing actual microseisms, but the larger the risk of declaring false events. Because the search window moves one sample at a time, in general there is not only one, but a certain number of contiguous windows that contain, at least partially, the microseism (see Fig. 5). Then, and in order to uniquely declare the actual microseism, we follow the criterion that is summarized below and is illustrated in Fig. 6:

1. All the contiguous windows that meet the above requirement to declare a microseism are stored (Fig. 6a shows the first and last ones).
2. A larger window is generated from the union of all contiguous windows that detected a microseism (Fig. 6b, green).
3. Finally, the large window is shortened as much as possible without leaving picks outside (Fig. 6b, red).

This shortened window is assumed to contain the microseism and all the arrival times for each trace where the event was detected. Afterwards, this final window may be visually inspected by an analyst to

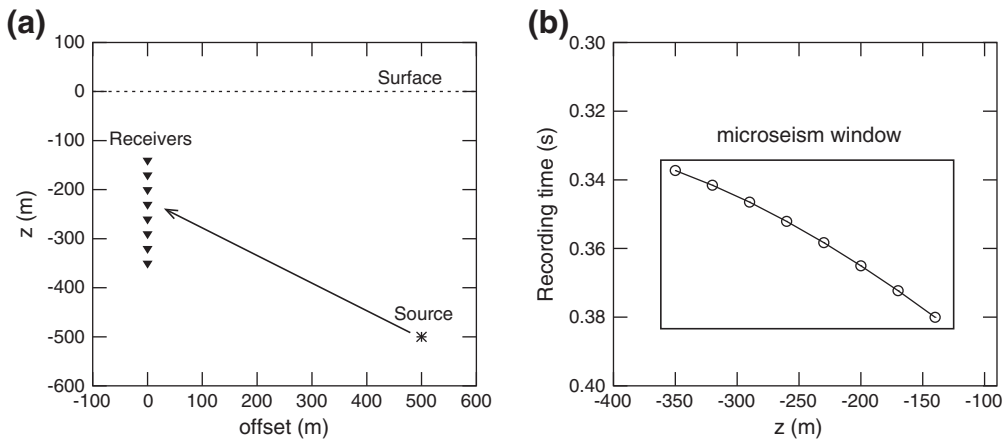

Fig. 4. (a) Typical acquisition geometry. (b) Expected arrival times aligned along a hyperbola.

decide, with the aid of the confidence indicator described below, whether the arrival times shall be corrected or not. Clearly, this is one small task considering the work that would require analyzing a complete microseismicity record of 2 or 3 h of duration, in which often only a few tens of microseisms are found. It is worth mentioning that this multi-channel strategy also contributes to increase the reliability of the picks and decrease the risk of false alarms.

2.4. Confidence indicator

To complete the description of the methodology, let us introduce a confidence indicator for the microseisms' declaration:

$$P[\%] = \left[\frac{1}{3}\sum_{k=1}^{3}\left(\frac{M^k_{\text{picks}}}{M}\right)^2\right]^{1/2} \times 100\%, \tag{9}$$

where M^k_{picks}, $k = 1, 2, 3$ represents the number of traces with picked events in each of the x-, y- or z-component, respectively, and M is the number of channels per component. In other words, P is the quadratic mean of the three M^k_{picks}/M ratios.

Note that if a microseism is detected within the search window in all the channels for each component, P will take a value of 100%. On the other hand, if the microseism is detected by the minimum condition (i.e. only in half of the channels of one of the three components), P will take a value of 28.9%. Also, if the microseism is detected in half of the channels of each component, P will be 50%, whereas P will be 57.7% if the microseism is detected in all the channels of one component and in none of the other two. The latter case may occur when the polarization pattern is such that the signal arrives polarized in one component only, and with high signal-to-noise ratio. Thus, the proposed quadratic mean considers properly this situation, assigning relatively high confidence values to the detected event. For those microseisms with P lower than 50%, the lower the P values are, the more attention

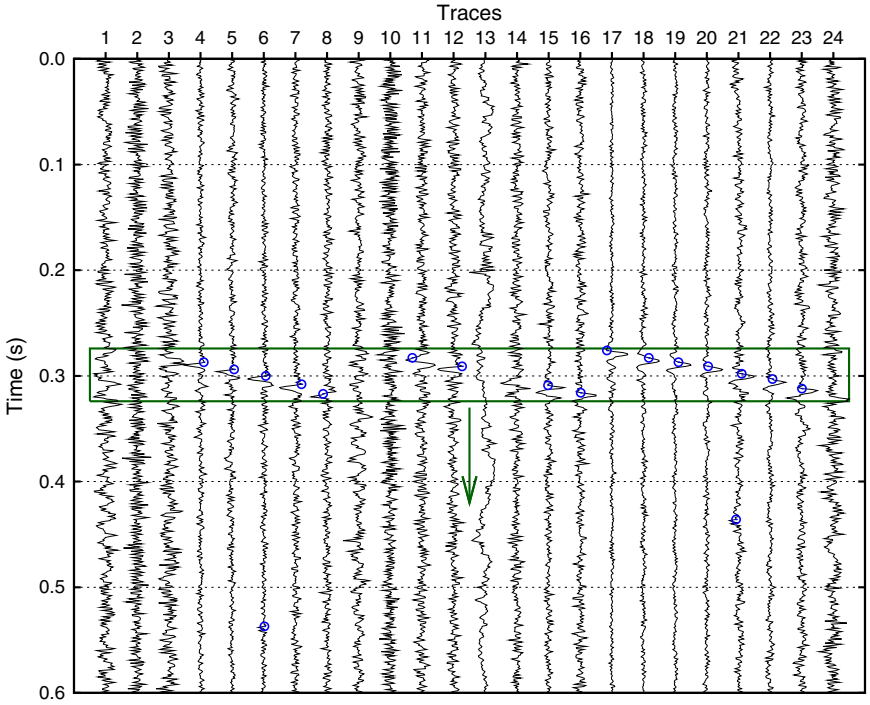

Fig. 5. Moving window used to detect the microseism (green). The window moves sample-by-sample in time and it is used to count the number of events within it. The picks (blue dots) were obtained using the MAM. (For interpretation of the references to color in this figure legend, the reader is referred to the web version of this article.)

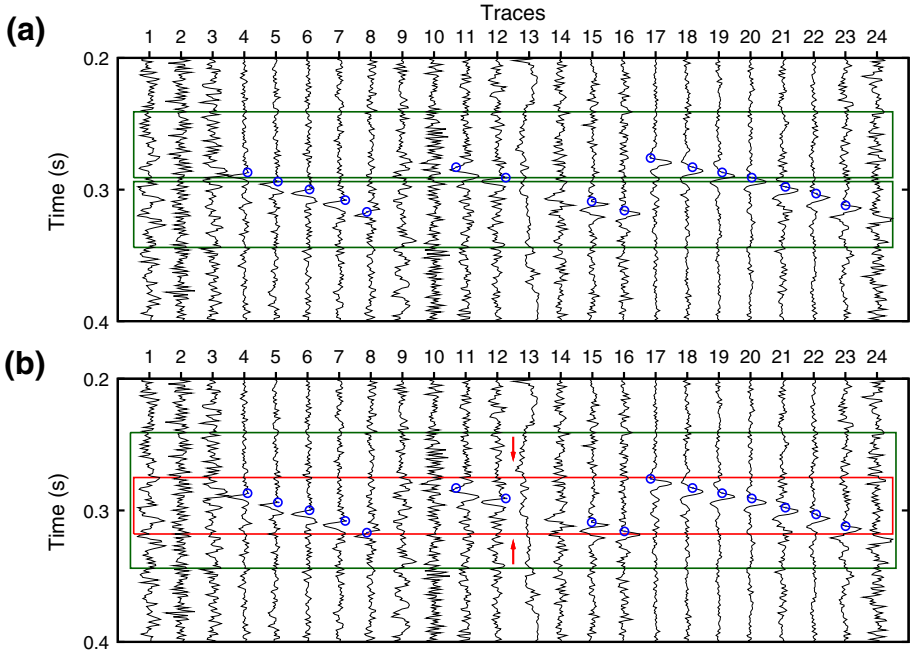

Fig. 6. Multi-trace strategy used to determine the shortest window that contains the microseism. (a) The first and last windows detecting the microseism (green). (b) The union of all contiguous moving windows yields a larger window (green). The larger window is shortened to define the shortest window that delimits the microseism (red). The picks (blue dots) were obtained using the MAM. (For interpretation of the references to color in this figure legend, the reader is referred to the web version of this article.)

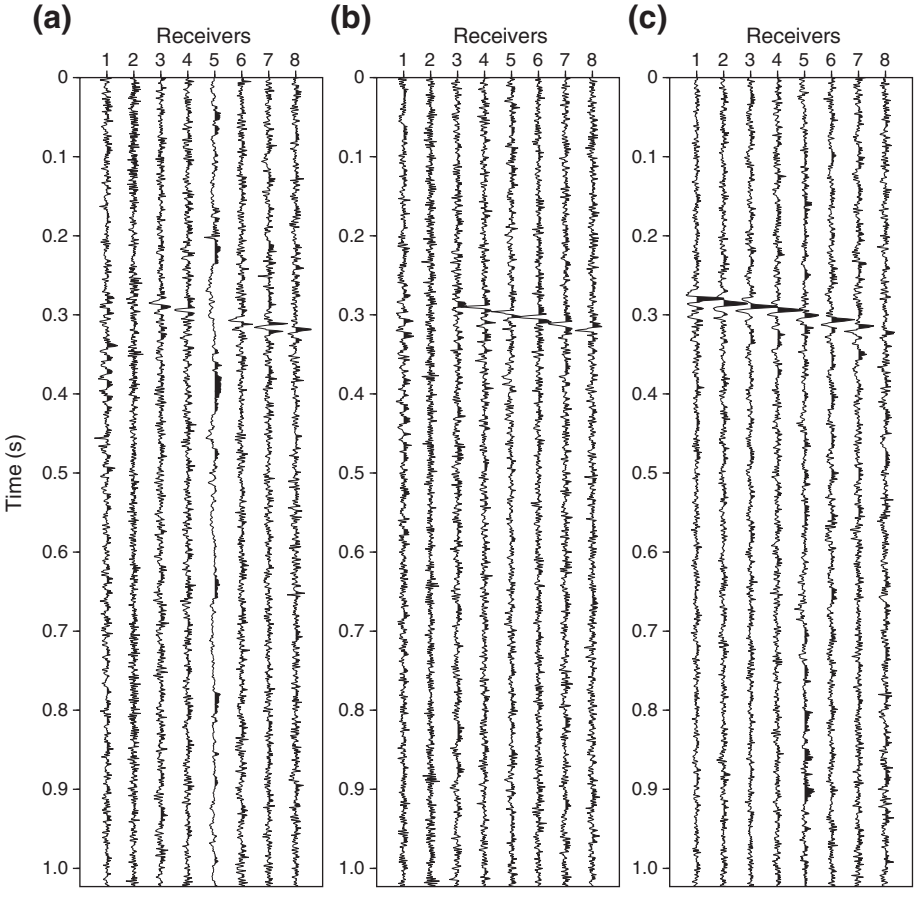

Fig. 7. Field record 1 (regular signal-to-noise ratio). (a) *x*-component, (b) *y*-component, and (c) *z*-component.

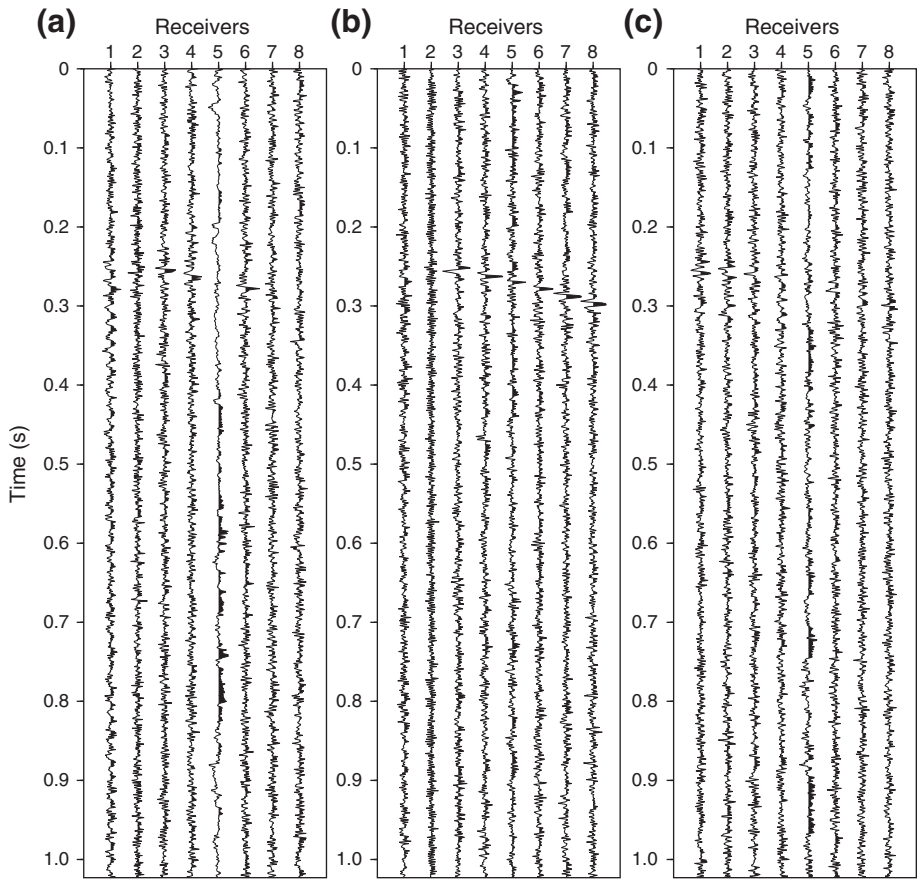

Fig. 8. Field record 2 (low signal-to-noise ratio). (a) *x*-component, (b) *y*-component, and (c) *z*-component.

the analyst shall pay regarding whether the detected microseism is a false positive or not.

3. Data and results

The two field records we selected to illustrate the methods were acquired in a monitor well located 500 m away from the extraction well using a vertical array of 8 triaxial receivers spaced 30 m. The same geometry was used in the synthetic example shown in Fig. 4a. Under these circumstances, and assuming that subsurface velocities do not vary too rapidly, microseisms' arrival times align approximately as low-curvature hyperbola, as we have already shown. The search window length was set equal to 50 ms for both datasets, following the criteria explained in the methodology description. Usually, microseismic data are recorded continuously from the very beginning of the injection process up to a few hours, and traces are then stored in small periods of time (e.g. 10 s). For simplicity and in order to illustrate the proposed method, we considered 1 s time windows containing a single microseism.

The first record, that exhibits a regular signal-to-noise ratio, is displayed in Fig. 7. The three components are shown in three independent panels in order to better appreciate the hyperbolas corresponding to the events. The microseism arrival can be seen between 270 ms and 330 ms, approximately. The arrival is particularly clear in the *z*-component, in most channels of the *y*-component, and, to a lesser extent, in the *x*-component. The fifth channel of the *x*-component, for example, seems to have some type of problem and contains no useful information.

The second record, that exhibits a low signal-to-noise ratio, is displayed in Fig. 8. There is an event between 240 and 300 ms, clearly visible in the *y*-component, barely distinguished in the *x*-component, and hardly detected (except by a well-trained observer) in the *z*-component. Again, the channel 5 of the *x*-component shows some problem. It is not surprising that an event which shows clearly in a given component could be indistinguishable in another, because this will depend on the polarization with which the wave arrives to the geophones.

Table 1 summarizes the parameters used for the trace-by-trace analysis (the same parameters were used for both field data records). The window lengths were set according to the expected microseismic signal period, which is about 10 ms. Recall that MAM and ESM share the same window scheme that was illustrated in Fig. 2b. For them, T_{STA} was set equal to half a period of the expected signal (i.e., 5 ms), whereas T_{LTA} was set equal to 50 ms. The Hanning window length was set to 10 ms for the three autopickers. On the other hand, the threshold value *THR* used to declare an event depends on the sensitivity of the attribute being used. Thus, *THR* must be tuned for each algorithm and can be used to control the number of events that are picked in a given trace: the smaller the *THR*, the greater the number of picked events (and vice versa).

Once the trace-by-trace picking was done, the multi-channel strategy was applied. The microseism was detected in both records using the picks obtained by the three automatic phase picker algorithms. In Table 2 we show the confidence indicators for the detected microseisms

Table 1
Parameters used in the trace-by-trace process.

Parameter	ESM	MAM	MBKM
T_{STA} (ms)	5	5	–
T_{LTA} (ms)	50	50	–
T_{Han} (ms)	10	10	10
THR	2.5	6.0	5.0

Table 2
Confidence indicator of the detected microseismic events.

	ESM	MAM	MBKM
Record 1	73,95%	68,47%	71,81%
Record 2	39,53%	29,76%	38,86%

for both records. The microseism of record 1 (regular signal-to-noise ratio) was detected in most of the traces using the different autopickers, which is reflected in the high values of *P*. On the other hand, although in record 2 (low signal-to-noise ratio) the microseism was also detected using the three trace-by-trace algorithms, the confidence levels are from moderate to low, because of the polarization in the *y*-component.

In Fig. 9 we show the final windows and the picks obtained for record 1 using each of the three autopickers. Clearly, the high values of *P* are explained by the fact that ESM and MBKM detected the event in 17 out of 24 traces (Fig. 9a and c), while MAM in 16 out of 24 (Fig. 9b). Particularly, regarding the *z*-component, the three methods picked the event either in the 8 channels (ESM) or in 7 (MAM and MBKM). These good results are achieved in spite of the background noise present in the data, which is not negligible. Note that for some traces it is very difficult (if not impossible) to detect the arrival by visual inspection (see traces 1, 2, 3, 9 and 10 in Fig. 9).

The automatic detection of the microseism in record 2 (Fig. 8) presents a greater challenge, for the signal-to-noise ratio is much lower. In the *z*-component (traces 17 to 24), the signal arrival is completely masked by the noise. In addition to the problems on channel 5, channels 1 and 2 for the *x*-component and also channel 10 are very noisy. As a consequence, after the trace-by-trace picking process, the event could only be detected in a few traces (see blue dots in Fig. 10). Even so, the method based on the three proposed alternatives for the first step managed to automatically detect the microseism after following the multi-trace strategy described previously (see red windows in Fig. 10). Note that confidence values are low (29–40%) because the microseism is detected due to the *x*-component, where only 4 or 5 arrivals were picked. However, it is important to remark that the method succeeded in its main task, which is to detect the presence of microseism without declaring a false event. In such a case, where the confidence values are low, the microseism window could be afterwards isolated in order to pick the arrivals in the other channels manually.

In regard to the actual times of the arrivals, notice that in all cases they were automatically picked with remarkable precision, as shown in Figs. 9 and 10. Although we did not use a homogeneous approach to define the exact time of the signal onset in each trace, the obtained times correspond approximately to the central lobe of signal arrival.

4. Discussion

The single-trace picking algorithms used in the first step are very simple and easy to apply, for the number of parameters required to "tune" them is minimum. Except for the threshold, which is used to control the sensibility of the individual trace-by-trace pickers, the selection of the remaining parameters relies on the expected period of microseismic arrivals (see Table 1). This is an advantage over other methods, since the parameter selection is crucial for the good performance of the autopickers.

According to the results shown in Figs. 9 and 10, and those summarized in Table 2, it is difficult to favor one picker over the other. A close inspection of the results reveals that, for some traces, the ESM tends to pick the events slightly before their actual arrival times. Besides, comparing Figs. 1b, 2b and 3b, it can be argued that the ESM is less sensible to the signal arrival than the MAM and MBK, which show more prominent peaks at different times that might be interpreted as additional arrivals. But the implementation of the Hanning filter contributes to level

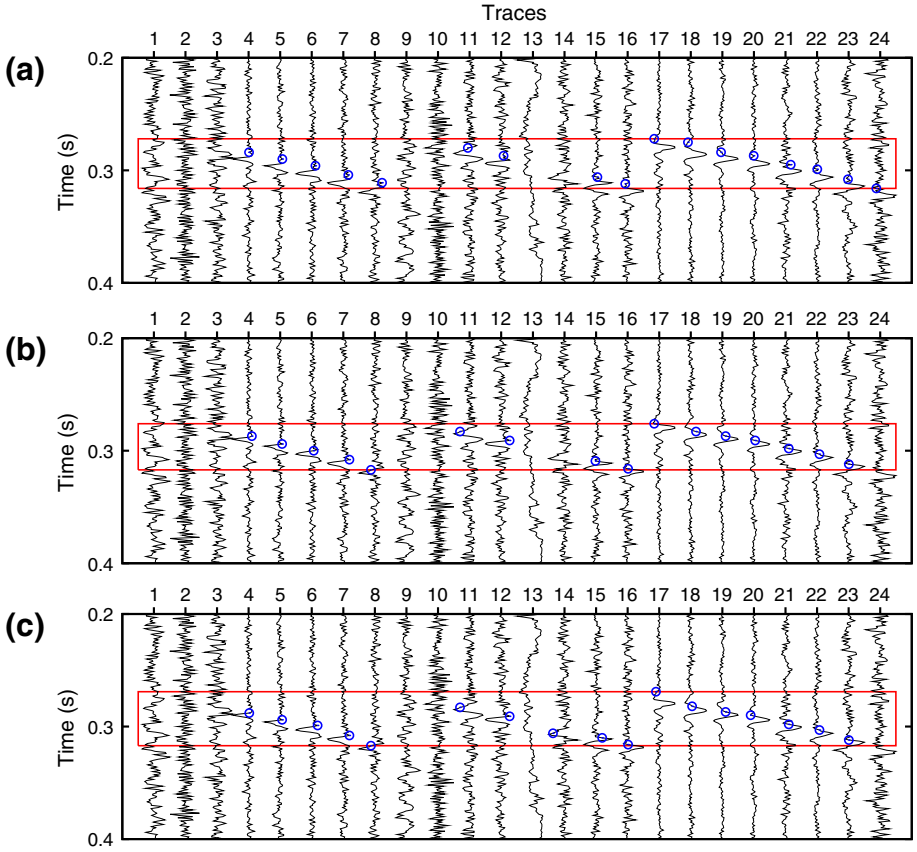

Fig. 9. Trace-by-trace picks (blue dots) using (a) ESM, (b) MAM, and (c) MBKM. Data correspond to record 1 (Fig. 7). The red rectangles represent the final windows after applying the multi-trace strategy to detect the microseism. (For interpretation of the references to color in this figure legend, the reader is referred to the web version of this article.)

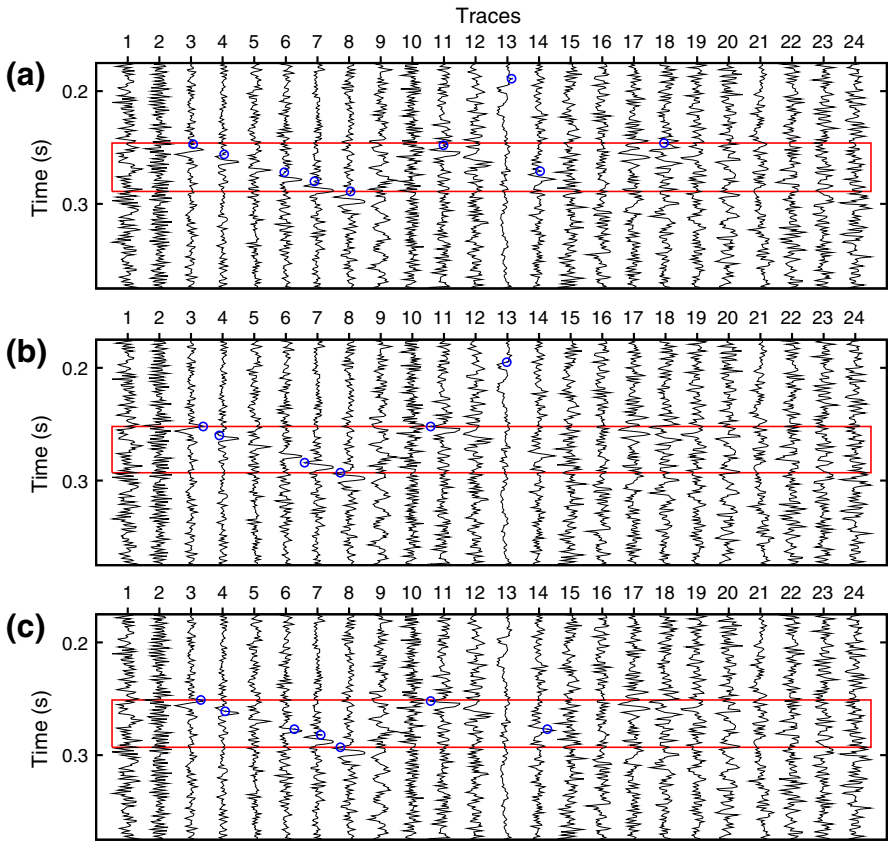

Fig. 10. Trace-by-trace picks (blue dots) using (a) ESM, (b) MAM, and (c) MBKM. Data correspond to record 2 (Fig. 8). The red rectangles represent the final windows after applying the multi-trace strategy to detect the microseism. (For interpretation of the references to color in this figure legend, the reader is referred to the web version of this article.)

the sensibility of the three autopickers, thus avoiding the detection of spurious events when dealing with very noisy data, as is the case of microseismic records. In this sense, the MAM and MBKM proposed in this paper represent novel algorithms for processing microseismic data.

The results depicted in Figs. 9 and 10, and those summarized in Table 2, also show that (1) the trace-by-trace picking process is very accurate, and (2) the multi-channel strategy not only succeeds in detecting the microseismic occurrences, but also contributes to prevent the declaration of false events. Further, the confidence indicator associated with any detected event can be used to help the analyst to make a decision in difficult situations. The multi-channel strategy is somewhat controlled by the search window length, a parameter that should be selected so as to encompass any expected microseismic event, as illustrated in Fig. 4b. Once this parameter is set (we used a 50 ms search window in all the cases), the "search" window is automatically adjusted to isolate the microseism, as illustrated in Fig. 6b. This simple process is very robust because it leads to the declaration of the event irrespective of whether it is partially present in one of the components (Fig. 10) or in all (Fig. 9).

5. Conclusions

We described a new method to process borehole microseismic data aimed to automatically detect and pick microseismic arrivals. The processing is carried out in two steps. First, three single-trace picking algorithms borrowed and adapted from earthquake seismology are implemented to search for potential microseismic arrivals along each trace of the data. Next, a multi-channel strategy is devised to assess the presence of a microseism. A confidence indicator is also proposed to associate a probability to each detected microseism.

Both the Modified Allen's method (MAM) and the Modified Baer and Kradolfer's method (MBKM) introduced in this paper performed very well when tested with noisy microseismic data. The multi-channel strategy is based on the quasi-horizontal alignment assumption of the microseismic arrivals, and represents a reliable method to detect the events automatically with very low false positive rates.

Results after applying the method to moderate and poor-quality field data examples demonstrate that the proposed automatic technique is robust and accurate. Furthermore, because of its simplicity and effectiveness, the method can be used with a relatively high confidence to process raw microseismic data on the fly, a key issue for current applications.

Acknowledgments

This work was partially supported by the Agencia Nacional de Promoción Científica y Tecnológica (PICT-2010-2129). We are highly grateful to Daniel Lorenzo for sharing valuable information and also for fruitful discussions during the preparation of this manuscript.

References

Allen, R., 1978. Automatic earthquake recognition and timing from single traces. Bulletin of the Seismological Society of America 68, 1521–1532.
Allen, R., 1982. Automatic phase pickers: their present use and future prospects. Bulletin of the Seismological Society of America 72, S225–S242.
Baer, M., Kradolfer, U., 1987. An automatic phase picker for local and teleseismic events. Bulletin of the Seismological Society of America 77, 1437–1445.
Chen, Z., Stewart, R., 2006. A multi-window algorithm for real-time automatic detection and picking of p-phases of seismic events. CREWES Research Report, 18 15.1–15.9.
Duncan, P.M., 2012. Microseismic monitoring for unconventional resource development. Geohorizons 26–30.
Earle, P., Shearer, P., 1994. Characterization of global seismograms using an automatic-picking algorithm. Bulletin of the Seismological Society of America 84, 366–376.
Kendall, M., Maxwell, S., Foulger, G., Eisner, L., Lawrence, Z., 2011. Special section. Microseismicity: beyond dots in a box — introduction. Geophysics 76, WC1–WC3.
Maxwell, S., 2011. What does microseismic tell us about hydraulic fractures? SEG Expanded Abstracts 1565–1569.

Maxwell, S., Urbancic, T., 2001. The role of passive microseismic monitoring in the instrumented oil field. The Leading Edge 20, 636–639.
Munro, K., 2004. Automatic event detection and picking of P-wave arrivals. CREWES Research Report, 16 12.1–12.10.
Oye, V., Zhao, P., Lecomte, I., Braathen, A., Olaussen, S., 2012. Microseismic monitoring and velocity model building at the Longyearbyen CO_2-Lab, Svalbard. In: EGU (Ed.), Geophysical Research Abstracts. European Geophysical Union, p. 12933.
Sabbione, J.I., 2012. Algoritmos matemáticos y computacionales para la detección automática de señales sísmicas. (Ph.D. thesis) Universidad Nacional de La Plata, La Plata, Argentina.
Sabbione, J.I., Velis, D.R., 2012. An automatic method for microseismic events detection based on earthquake phase pickers. SEG Expanded Abstracts. 1–5.
Shemeta, J., Anderson, P., 2010. It's a matter of size: magnitude and moment estimates for microseismic data. The Leading Edge 29, 296–302.
Vera-Rodriguez, I., Bonnar, D., Sacchi, M.D., 2011. Improvements in microseismic data processing using sparsity and non-linear inversion constraints. CSEG Recorder 24–28.
Verdon, J., 2011. Microseismic monitoring and geomechanical modeling of CO_2 storage in subsurface reservoirs. Geophysics 5, Z102.
Wong, J., Han, L., Bancroft, J., Stewart, R., 2009. Automatic time-picking of first arrivals on noisy microseismic data. CSEG Conference Abstracts.